



Production of new neutron-rich isotopes with $92 \leq Z \leq 100$ in multinucleon transfer reactionsXiao Jun Bao (包小军)^{1,*}, Shu Qing Guo (郭树青)^{2,†} and Peng Hui Chen (陈鹏辉)³¹*Department of Physics, Hunan Normal University, Changsha 410081, China*²*College of Physics and Optoelectronic Engineering, Shenzhen University, Shenzhen 518060, China*³*College of Physics Science and Technology, Yangzhou University, Yangzhou 225009, China*

(Received 16 October 2021; revised 20 December 2021; accepted 1 February 2022; published 17 February 2022)

To explore the optimum conditions for producing new neutron-rich isotopes in the range $92 \leq Z \leq 100$ by multinucleon transfer reactions, $^{86}\text{Kr} + ^{248}\text{Cm}$, $^{129}\text{Xe} + ^{248}\text{Cm}$, $^{132}\text{Xe} + ^{248}\text{Cm}$, $^{136}\text{Xe} + ^{248}\text{Cm}$ and $^{238}\text{U} + ^{248}\text{Cm}$ systems with bombarding energies around their respective Coulomb barriers are investigated within an improved dinuclear system (DNS) model, combined with the statistical GEMINI++ model. The calculated production cross sections are in a good agreement with experimental data. It is found that, compared with projectiles ^{86}Kr and ^{136}Xe , the projectile ^{238}U can produce larger cross sections of neutron-rich nuclei of interest by bombarding the actinide target ^{248}Cm . Actinide projectile-target combination seems to be encouraging for the production of neutron-rich isotopes with $92 \leq Z \leq 100$.

DOI: [10.1103/PhysRevC.105.024610](https://doi.org/10.1103/PhysRevC.105.024610)**I. INTRODUCTION**

In recent years, much interest has been focused on heavy-ion induced multinucleon transfer (MNT) reactions for synthesizing neutron-rich transactinide and nuclides along the closed $N = 126$ neutron shell closure [1–4]. However, almost all known neutron-rich actinides are produced by neutron capture, the direct reaction with long-lived neutron-rich actinides, or light charged particle induced reaction [5]. These methods seem to fail when synthesizing new, more neutron-rich nuclides [5,6]. In addition, heavy-ion fusion evaporation reactions based on stable beams produce relatively neutron-deficient products owing to the bend of the valley of β stability in the direction of neutron excess with increasing proton number. Thus, there are no combinations of stable nuclei that may be used to produce neutron-rich transuranium nuclei in fusion evaporation reactions.

Up to now, multinucleon transfer processes in near-barrier collisions seem to be the only possibility allowing us to produce and explore neutron-rich transuranium nuclei. A pioneering experiment of a multinucleon transfer reaction had been carried out to synthesize a new neutron-rich ^{244}Np isotope with heavy ion ^{136}Xe bombarding a ^{244}Pu actinide target [7]. In the experiment [7], the isolation and the identification of two new β -decaying neutron-rich isotopes, ^{243}Np and ^{244}Np , were reported. It was found that multinucleon transfer reactions could provide a feasible way to produce other unknown actinides.

Recently, about 100 residual nuclei with proton numbers between $Z = 82$ and $Z = 100$ were observed by using the multinucleon transfer reaction $^{48}\text{Ca} + ^{248}\text{Cm}$ which produced

five new neutron-deficient isotopes: ^{216}U , ^{219}Np , ^{223}Am , ^{229}Am , and ^{233}Bk [8]. Before the experiment mentioned above, the fusion evaporation reaction was considered to be the only feasible method to produce neutron-deficient actinide isotopes [5,6].

It is worth noting that with the increase of transferred nucleons, the production cross section of nuclides whose mass exceeds the target decreases rapidly [9–15]. In addition, although various theoretical approaches have been developed to explore the multinucleon transfer process [16–47], systematic studies on estimating the optimum projectile-target combinations for the multinucleon transfer products have not been well performed so far. Therefore, to study the dependence of actinide-nuclide production on the projectile and target in the heavy-ion reaction, we hope to explore the conditions required to maximize the yield of nuclides of interest and further understand the transfer process.

Based on the semiphenomenological treatment of the dissipation process of the heavy-ion collision, the production cross section of new isotopes in the multinucleon transfer reaction is theoretically estimated in the framework of the improved dinuclear system model, where the dynamic deformations of interacting nuclei are taken into account [48]. Our confidence in such estimates is based on the remarkable success in analyzing dissipative collisions in different projectile-target combinations and bombarding energies [47–52].

In general, projectiles with higher values of N/Z should be more favorable in producing neutron-rich primary and final fragments. The main purpose of this work is to try to understand the above mentioned aspect, and to evaluate what combination is more conducive to the production of new actinide isotopes. The present study is a part of our continuous research, and some efforts are made to systematically study various projectile-target combinations as in our previous work, to strengthen the current understanding of transfer

*baoxiaojun@hunnu.edu.cn

†guosq@szu.edu.cn

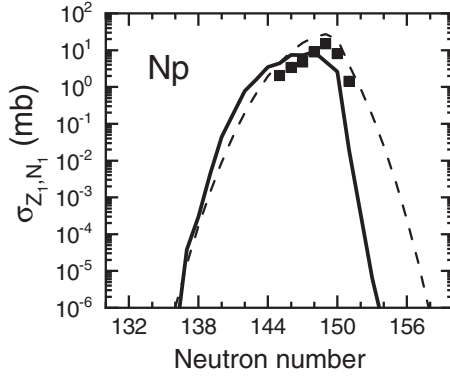


FIG. 1. Production cross sections of Np isotopes in the $^{136}\text{Xe} + ^{244}\text{Pu}$ reaction at $E_{c.m.} = 536.15$ MeV. The calculated primary and final products are denoted by the dashed and solid lines, respectively. The measured cross sections are taken from Ref. [7].

reactions, and to shed light on the prospects for the synthesis of new isotopes with $92 \leq Z \leq 100$.

II. THEORETICAL FRAMEWORK

The production cross section of a primary product in the multinucleon transfer reaction is written as a sum over all

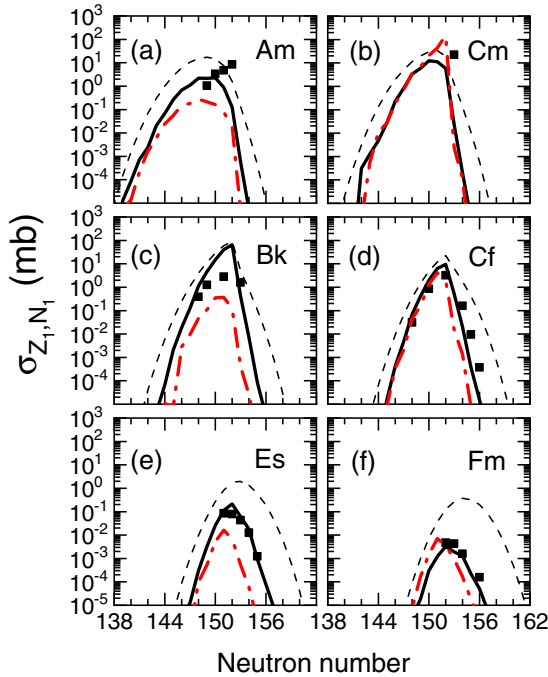


FIG. 2. Calculated primary (dashed) and final (solid) fragments in the $^{86}\text{Kr} + ^{248}\text{Cm}$ reaction at incident energy $E_{c.m.} = 386.10$ MeV. The red dash-dotted lines denote the distributions of final fragments obtained by taking the pairing energy into account, but not shell damping effect. The measured cross sections are taken from Ref. [11].

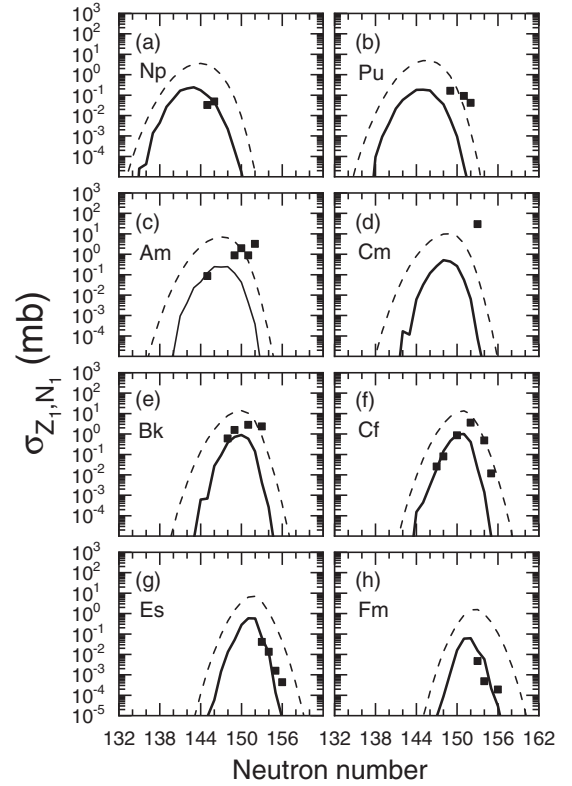


FIG. 3. The production cross sections of primary (dashed) and final (solid) products of the $^{129}\text{Xe} + ^{248}\text{Cm}$ reaction at bombarding energy $E_{c.m.} = 513.10$ ($1.05V_{\text{Bass}}$). The measured cross sections are taken from Ref. [64].

partial waves J [50],

$$\sigma_{Z_1, N_1}^{\text{pri}}(E_{c.m.}) = \frac{\pi \hbar^2}{2\mu E_{c.m.}} \sum_J (2J+1) T(E_{c.m.}, J) \times \sum_{\beta_1} \sum_{\beta_2} P(Z_1, N_1, \beta_1, \beta_2, J, \tau_{\text{int}}), \quad (1)$$

where the penetration coefficient $T(E_{c.m.}, J)$ is estimated to be 1 when the incident energy is higher than the interaction barrier. The interaction time τ_{int} in Eq. (1) determines how far the system travels along the potential energy surface, and the interaction time τ_{int} in the dissipative process of two colliding nuclei is determined by using the deflection function method [53–56].

The rearrangement process of mass and charge between the projectile-like and target-like fragments is governed by the potential energy surface of the dinuclear system; the distributions of primary fragments can be better determined if the underlying balance between dynamical and static driving forces of dissipative heavy-ion collisions is understood [49]. On one hand, the DNS should be gradually deformed due to strong nuclear and Coulomb interactions between its nuclei. Deformations of the reaction partners are no longer the ground

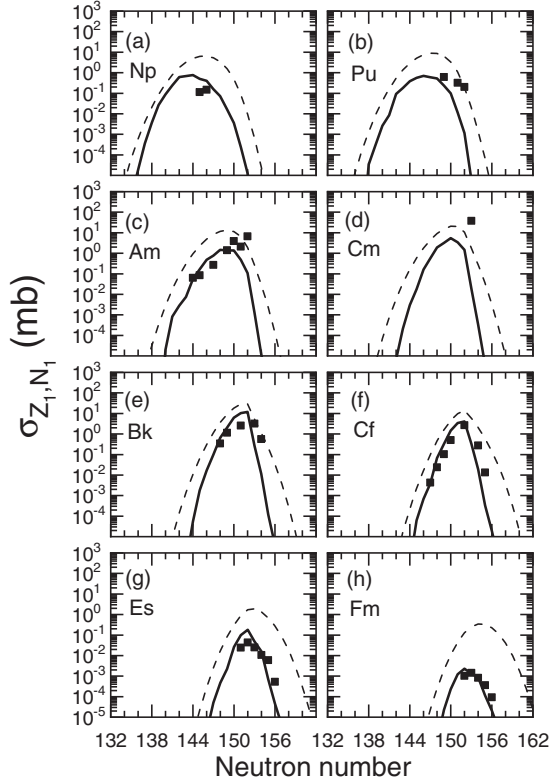


FIG. 4. Same as the Fig. 3, but for the $^{132}\text{Xe} + ^{248}\text{Cm}$ reaction at bombarding energy $E_{c.m.} = 525.36$ MeV ($1.08V_{\text{Bass}}$). The measured cross sections are taken from Ref. [64].

$$\begin{aligned}
 U(N_1, Z_1, N_2, Z_2, R_{\text{cont}}, \beta_1, \beta_2, J) = & V_{\text{CN}}(N_1, Z_1, N_2, Z_2, R_{\text{cont}}, \beta_1, \beta_2) + V_{\text{rot}}(N_1, Z_1, N_2, Z_2, R_{\text{cont}}, \beta_1, \beta_2, J) \\
 & + B_{LD}^1(N_1, Z_1, \varepsilon_1^*) \prod_{k \geq 2} (1 + b_k \beta_k^2) + E_{\text{shell}}^1(N_1, Z_1, \beta) \exp(-\gamma_D \varepsilon_1^*) + B_{LD}^2(N_2, Z_2, \varepsilon_2^*) \prod_{k \geq 2} (1 + b_k \beta_k^2) \\
 & + E_{\text{shell}}^2(N_2, Z_2, \beta) \exp(-\gamma_D \varepsilon_2^*),
 \end{aligned} \quad (3)$$

where β_1 and β_2 represent quadrupole deformations of the two fragments. The nucleon transfer process is assumed to occur at $R_{\text{cont}} = R_1(1 + \beta_1 Y_{20}(\theta_1)) + R_2(1 + \beta_2 Y_{20}(\theta_2)) + 0.5$ fm, with $R_i = 1.16A_i^{1/3}$. The nucleus-nucleus interaction potential $V_{\text{CN}}(N_1, Z_1, N_2, Z_2, R_{\text{cont}}, \beta_1, \beta_2)$ between two interacting nuclei of the DNS configuration is the sum of the nuclear interaction potential V_{N} obtained from the folding integral of a zero-range nucleon-nucleon interaction and the Coulomb interaction potential V_{C} calculated by Wong's formula [57–59]. The rotational energy $V_{\text{rot}} = \hbar^2 J(J+1)/I_{\text{tot}}$, where the moment of inertia I_{tot} is approximated by its rigid-body value.

The ε_i^* in Eq. (3) is allocated from the local energy of the DNS, according to the mass number A_i , and the damping factor means the speed of washing out the shell correction against the excitation energy. In the present work $\gamma_D^{-1} = 20$ MeV is adopted in accordance with the general range 18–25 MeV. The pairing energy term is included in the liquid-drop energy of a spherical nucleus, $B_{LD}^i(N_i, Z_i, \varepsilon_i^*)$ [60]. As the

state values. On the other hand, the characteristic that the shape of the nucleus tends to be spherical at high excitation energy (temperature effects) should be included.

In order to consider consistently the temperature effects and dynamical deformation on the potential energy surface, the quadrupole deformations β_1 and β_2 of projectile-like and target-like fragments are considered as two discrete variables, respectively [49]. The multinucleon rearrangement processes between the interacting projectile and target are described as a diffusion process by numerically solving a set of four-variable master equations in the corresponding four-variable potential energy surface. The time evolution of the probability distribution function $P(Z_1, N_1, \beta_1, \beta_2, t)$ for fragment 1 with Z_1, N_1, β_1 , and β_2 at time t is described by the master equations.

The mean transition probability and microscopic dimensions in the four-variables master equations are related to the local excitation energy. The local excitation energy ε^* is defined as

$$\begin{aligned}
 \varepsilon^*(J) = & E_x(J, t) - [U(N_1, Z_1, N_2, Z_2, R_{\text{cont}}, \beta_1, \beta_2, J) \\
 & - U(N_P, Z_P, N_T, Z_T, R_{\text{cont}}, \beta_{10}, \beta_{20}, J)],
 \end{aligned} \quad (2)$$

where the first term denotes dissipation energy $E_x(J, t)$ which is converted from the relative kinetic energy loss. The second term in Eq. (2) is the potential energy surface of the system, which is

underlying idea is that the paired nucleons must be separated to excite each component, the corresponding pairing energy should be excluded for calculating the level density or the state density in many Fermi-gas type models.

The total excitation energy of primary fragments can be expressed as $E_{\text{tot}} = E_{c.m.} - \text{TKE} + Q_{\text{gg}}$, where the total kinetic energy (TKE) is the sum of the Coulomb energy, nuclear energy, and radial kinetic energy at the exit channel. The Q_{gg} value corresponds to the reaction energy of the exit channel of interest.

The deexcitation process of the present work is simulated by the statistical model GEMINI++, and the calculation is carried out by using the default parameters of that model [61,62]. The production cross section of final fragments can be given as

$$\sigma_{Z_1, N_1}^{\text{fin}}(E_{c.m.}) = \sum_{Z'_1, N'_1, J'} \sigma_{\text{pri}}(Z'_1, N'_1, J') \times P(Z_1, N_1; Z'_1, N'_1, J'), \quad (4)$$

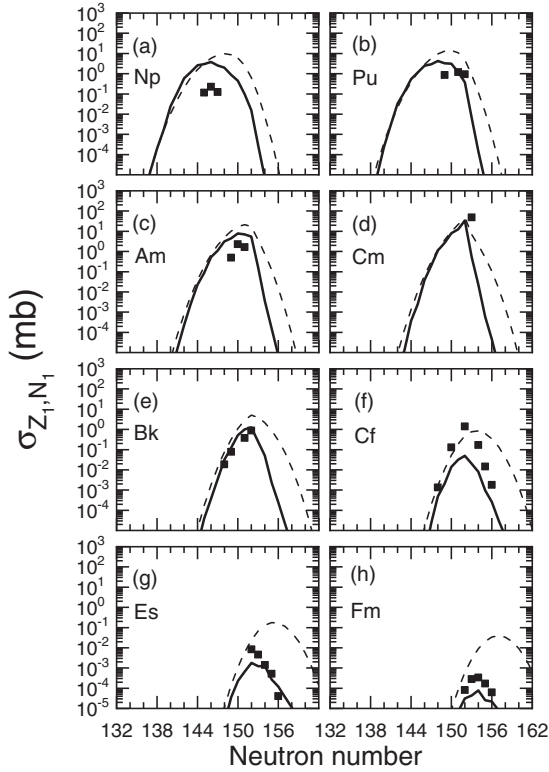


FIG. 5. Same as the Fig. 3, but for the $^{136}\text{Xe} + ^{248}\text{Cm}$ reaction at bombarding energy $E_{c.m.} = 519.89$ MeV ($1.07V_{\text{Bass}}$). The measured cross sections are taken from Refs. [64,65].

where $P(Z_1, N_1; Z'_1, N'_1, J')$ represents the decay probability. It is assumed that the sharing of the total excitation energy between the projectile-like fragments (PLFs) and target-like fragments (TLFs) are proportional to their masses, $E_{Z_1, N_1}^* = E_{\text{tot}}^* \times A_1 / (A_1 + A_2)$, where A_1, A_2 are the corresponding mass numbers. A pioneering experiment of multinucleon transfer reaction has been carried out. The reaction $^{136}\text{Xe} + ^{244}\text{Pu}$ at $E_{c.m.} = 536.15$ MeV ($1.11V_{\text{Bass}}$ [63]) was used to study the production mechanism and decay properties of the neutron-rich isotopes ^{243}Np and ^{244}Np . In Fig. 1 we show the measured production cross section of Np isotopes compared to the predictions of improved DNS plus GEMINI++ calculations. A good agreement between the calculated results and the experimental data [7] is shown.

III. NUMERICAL RESULTS AND DISCUSSIONS

The production cross sections of actinide isotopes in the multinucleon transfer reaction $^{86}\text{Kr} + ^{248}\text{Cm}$ at bombarding energy $E_{c.m.} = 386.10$ MeV ($1.15V_{\text{Bass}}$ [63]) are calculated by taking into account the damping shell energy but not pairing energy in the potential energy surface calculation, with the results shown by black solid lines in Fig. 2. It can be seen that the calculated production cross sections of Am, Cm, Bk, Cf, Es, and Fm isotopes are consistent with the experimental data. In addition, one can also see from Fig. 2 that the maximum cross sections of proton pickup channels from $+1p$ to

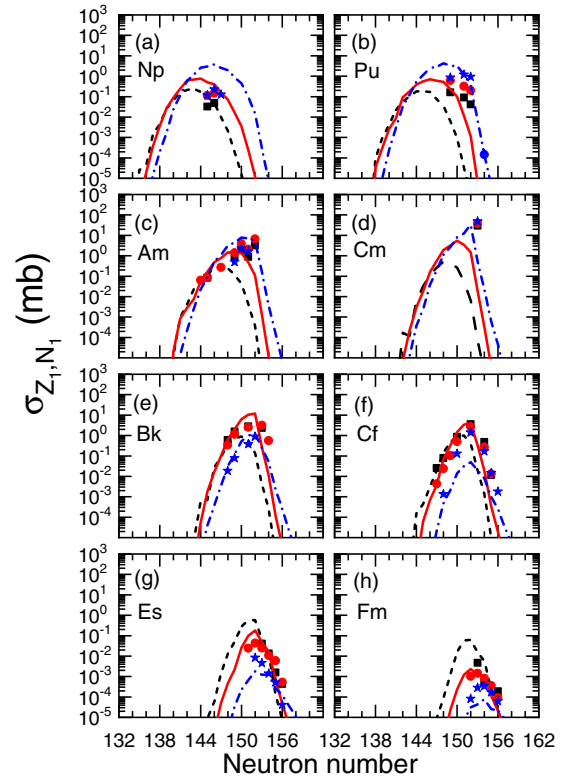


FIG. 6. The comparison of calculated (measured) production cross section of final fragments in $^{129}\text{Xe} + ^{248}\text{Cm}$, $^{132}\text{Xe} + ^{248}\text{Cm}$, and $^{136}\text{Xe} + ^{248}\text{Cm}$ reactions, with black dashed lines (squares), red solid lines (cycles), and blue dash-dotted lines (stars), respectively.

$+4p$ calculated by our model are in good agreement with the maximum observed experimentally.

The cross sections of primary fragments are shown by black dashed lines in Fig. 2. By comparing the yield distribution of primary fragments and final fragments, one can find that the branching ratio for neutron evaporation versus fission becomes very small with the increase of the number of transferred protons. Thus, the survival probability for superheavy nuclei might be suppressed.

For comparison, theoretical production cross sections considering the pairing energy but not the damping shell energy in the potential energy surface calculation are shown in Fig. 2 by red dash-dotted lines, and they are systematically underestimated, especially in odd proton transfer channels (Am, Bk, and Es isotopes).

From the perspective of transport models, the primary-fragment distribution is thought to be strongly influenced by the underlying potential energy surfaces. The shell and pairing effects of the nuclei affect the calculation of the potential energy surface. The primary yields are related to the local excitation energy or the potential energy surface. The most likely neutron and proton arrangement of products should occur when the density of states in the dinuclear system is the largest, which corresponds to a minimum of the potential energy in the dinuclear system. We find that the inclusion of ground state shell corrections and pairing energies of

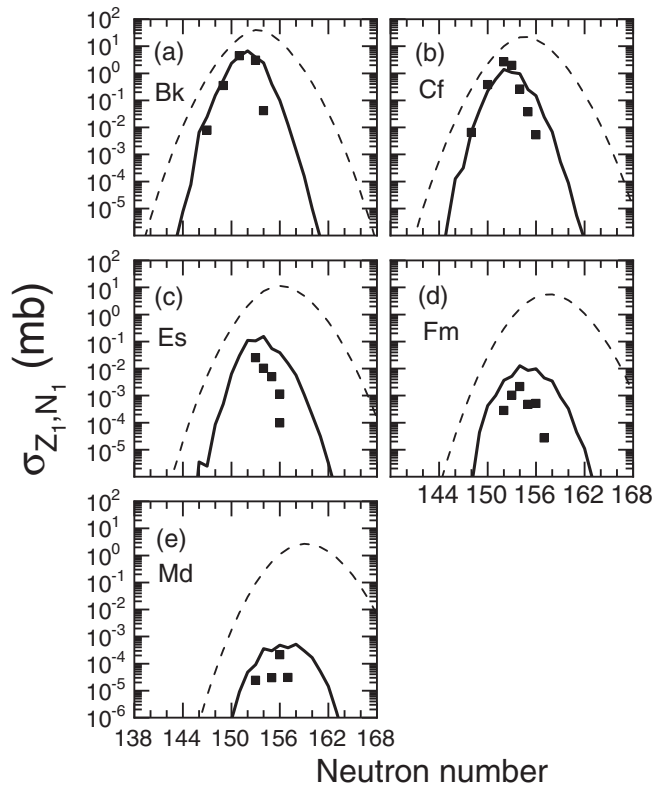


FIG. 7. Same as the Fig. 3, but for the $^{238}\text{U} + ^{248}\text{Cm}$ reaction at bombarding energy $E_{c.m.} = 898.7$ MeV. The measured cross sections are taken from Ref. [10].

projectile-like and target-like fragments to estimate the binding energies can affect the position of the minimum of the potential energy for a given Z .

Production cross sections of actinide nuclides in the reactions using different $^{129,132,136}\text{Xe}$ projectiles bombarding the same ^{248}Cm target are also calculated by the improved DNSplus GEMINI++ model. Figures 3–5 show the comparison between the experimental data (squares) and the calculated results of primary (dashed lines) and final (solid lines) products. It is found that the final product distribution changes greatly with the increase of the number of transferred protons, and the branching ratio of neutron evaporation versus fission decreases gradually. From the each panel of Figs. 3–5, it is found that the calculated results are relatively consistent with the experimental data. The peak position of the production distribution for a given Z is reasonably predicted. Therefore, the improved DNS model plus GEMINI++ can be used to predict quantitatively the evolution of the proton and neutron distributions when the steep gradient in the potential energy surface for the projectiles $^{129,132}\text{Xe}$ is involved.

Generally, projectiles with higher N/Z value should be more beneficial to produce neutron-rich primary and final fragments when bombarding the same target. In order to study the effect of the N/Z on the yield distribution of actinide nuclei, the production cross sections with three different projectiles bombarding the same ^{248}Cm target are shown in Fig. 6 for comparison. The production cross sections of below-target

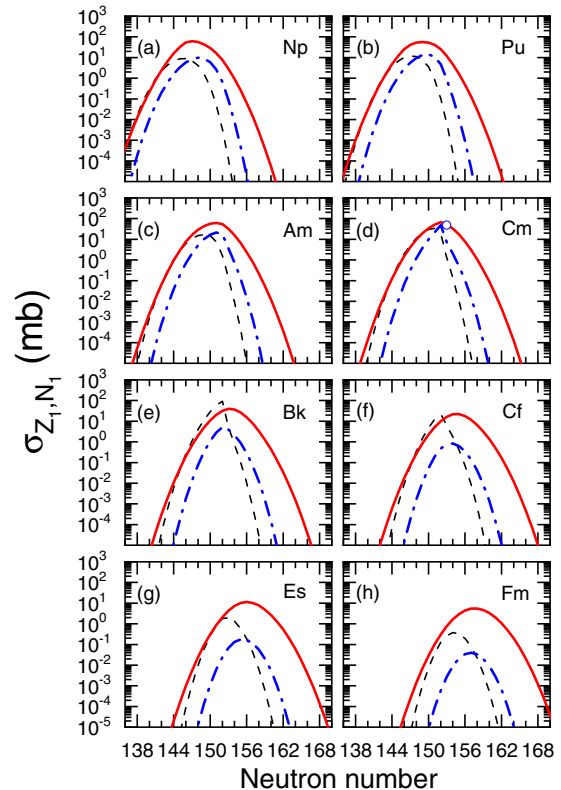


FIG. 8. Comparison of calculated production cross section of primary products in reactions $^{86}\text{Kr} + ^{248}\text{Cm}$ (black dashed), $^{136}\text{Xe} + ^{248}\text{Cm}$ (blue dash-dotted) and $^{238}\text{U} + ^{248}\text{Cm}$ (red solid).

Np, Pu, and Am isotopes with ^{129}Xe bombarding a ^{248}Cm target are about two orders of magnitude smaller than the ones with ^{136}Xe bombarding the same target. Meanwhile, the distribution of production cross section for a given Z seems to move towards smaller mass by using the more neutron-deficient projectiles. Therefore, the reaction with ^{129}Xe is more favorable for producing neutron-deficient isotopes, while ^{136}Xe is more favorable for neutron-rich ones.

It can be seen from Fig. 6 that the production of above-target nuclides is favored by using $^{129,132}\text{Xe}$ projectiles. The measured data of four isotopes (Bk, Cf, Es, and Fm) also show the increasing production cross section with the more neutron-deficient $^{129,132}\text{Xe}$ projectiles. The theoretical results of above-target isotopes seem to confirm the presence of a strong isospin driving force. This is consistent with the experimental study, showing that, due to the use of more neutron-deficient projectiles, the production of $Z > Z_{\text{target}}$ increases, while the production of $Z < Z_{\text{target}}$ decreases. The calculated production cross sections of three different projectiles $^{129,132,136}\text{Xe}$ bombarding the same target ^{248}Cm can be explained by the gradient difference of the potential energy surface at the injection point. This is because the location of the injection point on the potential energy surface directly affects the next transfer process. The most probable mass arrangement should occur when the density of states in the

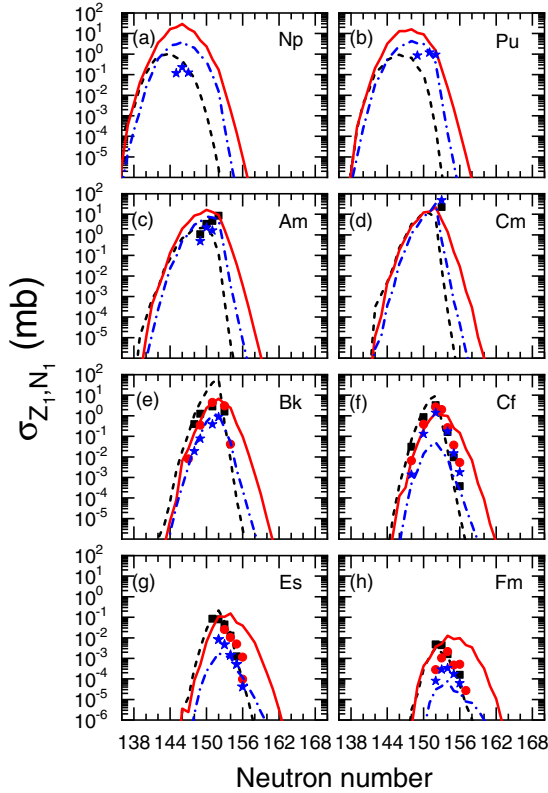


FIG. 9. Same as the Fig. 6, but for the respective $^{86}\text{Kr} + ^{248}\text{Cm}$, $^{136}\text{Xe} + ^{248}\text{Cm}$, and $^{238}\text{U} + ^{248}\text{Cm}$ reactions.

dinuclear system is the largest, which corresponds to a minimum of the potential energy in the system. We found that in the experiment with ^{136}Xe , the maximum of isotope distribution corresponds to the minimum of the potential energy surface, whereas in the experiment with ^{129}Xe and ^{132}Xe , the transfer of 2 to 3 protons is required to reach the minimum of the potential energy surface.

In order to further test our model, the theoretical cross sections of actinide production in damped collisions $^{238}\text{U} + ^{248}\text{Cm}$ at $E_{c.m.} = 898.7$ MeV are shown in Fig. 7. The experimental data denoted by squares are taken from the Ref. [10], while the theoretical primary and final products are denoted by dashed and solid lines, respectively. A good agreement between the theoretical and experimental cross sections of the isotopes of Bk and Cf can be shown in Fig. 7. However, the maximum values of Es, Fm, and Md isotopic distributions are systematically overestimated.

To study the influence of projectiles with different mass on the production cross section, we first compared the calculated isotope distribution of primary fragments in $^{86}\text{Kr} + ^{248}\text{Cm}$, $^{136}\text{Xe} + ^{248}\text{Cm}$, and $^{238}\text{U} + ^{248}\text{Cm}$ reactions, as shown in Fig. 8. We found that the distribution of the ^{238}U ($N/Z = 1.58$) induced reaction appeared to extend out to larger neutron numbers as compared to the ^{86}Kr ($N/Z = 1.39$) and ^{136}Xe ($N/Z = 1.51$) induced reactions. Figure 9 shows the corresponding production distribution of final fragments in reactions discussed above. In Figs. 8 and 9, it is found that the width of the isotope distribution of primary and final

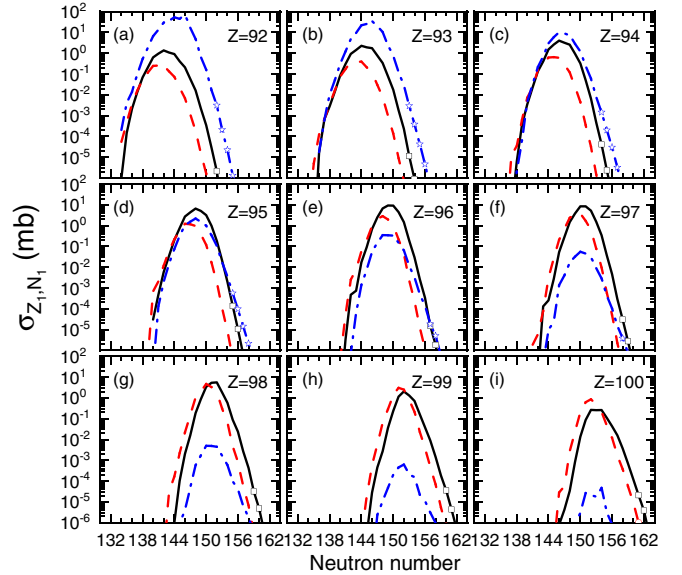


FIG. 10. Predicted production cross section of final isotopes in $^{248}\text{Cm} + ^{249}\text{Cf}$ (black solid), $^{249}\text{Cf} + ^{249}\text{Cf}$ (red dashed), and $^{238}\text{U} + ^{238}\text{U}$ (blue dash-dotted) reactions. New isotopes are denoted by open symbols.

fragments increases with the increase of the projectile mass. The large gain in production of the primary fragments could be largely compensated by the concurrent decrease in their survivability because of the much lower Q_{gg} values for heavier projectiles. For example, for the peak of the Fm isotope distribution, we obtain the average number of neutrons emitted in the respective $^{86}\text{Kr} + ^{248}\text{Cm}$ (two neutron), $^{136}\text{Xe} + ^{248}\text{Cm}$ (three neutron), and $^{238}\text{U} + ^{248}\text{Cm}$ (five neutron) systems. Compared with ^{86}Kr and ^{136}Xe projectiles, the neutron-rich products induced by the ^{238}U projectile have a relatively larger production cross section; this trend is quite encouraging for production of new neutron-rich isotopes with $92 < Z \leq 100$ using ^{238}U bombarding the actinide target.

The comparison mentioned above can be regarded as a representative example because the behavior of the production cross sections is similar to other projectile target combinations in the uranium region. By assuming that this holds true for all projectiles, we extended our extrapolations to different projectile-target combinations obtained from actinide nuclei. Figure 10 shows the predicted cross sections of final isotopes of $92 \leq Z \leq 100$ produced by the reactions of $^{248}\text{Cm} + ^{249}\text{Cf}$, $^{249}\text{Cf} + ^{249}\text{Cf}$, and $^{238}\text{U} + ^{238}\text{U}$. For new neutron-rich transuranium isotopes (open circles) with $92 \leq Z \leq 95$, the production of interest in the $^{238}\text{U} + ^{238}\text{U}$ reaction is larger than that in $^{248}\text{Cm} + ^{249}\text{Cf}$ or $^{249}\text{Cf} + ^{249}\text{Cf}$ reactions, while in the range $97 \leq Z \leq 100$ the production of interest in the $^{248}\text{Cm} + ^{249}\text{Cf}$ reaction is larger than that in the $^{249}\text{Cf} + ^{249}\text{Cf}$ or $^{238}\text{U} + ^{238}\text{U}$ reaction.

IV. SUMMARY

In summary, to search for the optimal conditions for synthesizing neutron-rich isotopes in the range $92 \leq Z \leq 100$, the improved DNS model combined with GEMINI++ is

adopted in multinucleon transfer reactions, with different projectile induced $^{86}\text{Kr} + ^{248}\text{Cm}$, $^{129}\text{Xe} + ^{248}\text{Cm}$, $^{132}\text{Xe} + ^{248}\text{Cm}$, $^{136}\text{Xe} + ^{248}\text{Cm}$, and $^{238}\text{U} + ^{248}\text{Cm}$ reactions, respectively. Our calculations are in good agreement with the experimental data. It is reasonable to use the improved DNS model plus GEMINI++ to study multinucleon transfer reactions. Larger cross sections of neutron-rich products are found by using the ^{238}U projectile, as compared to ^{86}Kr and ^{136}Xe projectiles; therefore, using projectile-target combinations with actinide nuclei is quite encouraging for the production of new neutron-rich isotopes with $92 \leq Z \leq 100$.

Productions of the final isotopes with $92 \leq Z \leq 100$ are predicted in the $^{248}\text{Cm} + ^{249}\text{Cf}$, $^{249}\text{Cf} + ^{249}\text{Cf}$, and $^{238}\text{U} + ^{238}\text{U}$ reactions.

ACKNOWLEDGMENTS

The work is supported by the National Natural Science Foundation of China (Grants No. 12175064, No. U2167203, No. 12105181, and No. 12105241), the Hunan Provincial Education Department (Key Project No. 20A290) and the NSF of Jiangsu Province (Grant No. BK20210788).

-
- [1] H. Freiesleben and J. V. Kratz, *Phys. Rep.* **106**, 1 (1984).
 [2] L. Corradi, G. Pollarolo, and S. Szilner, *J. Phys. G* **36**, 113101 (2009).
 [3] J. V. Kratz, W. Loveland, and K. J. Moody, *Nucl. Phys. A* **944**, 117 (2015).
 [4] F.-S. Zhang, C. Li, L. Zhu, and P. W. Wen, *Front. Phys.* **13**, 132113 (2018).
 [5] M. Thoennessen, *The Discovery of Isotopes: A Complete Compilation* (Springer, Berlin, 2016).
 [6] M. Thoennessen, *Nucl. Data Sheets* **118**, 85 (2014).
 [7] K. J. Moody, W. Bröchle, M. Brügger, H. Gäggeler, B. Haefner, M. Schädel, K. Sümmerer, H. Tetzlaff, G. Herrmann, N. Kafrell *et al.*, *Z. Phys. A* **328**, 417 (1987).
 [8] H. M. Devaraja, S. Heinza, O. Beliuskina, *et al.*, *Phys. Lett. B* **748**, 199 (2015).
 [9] M. Schädel, J. V. Kratz, H. Ahrens, W. Bröchle, G. Franz, H. Gäggeler, I. Warnecke, G. Wirth, G. Herrmann, N. Trautmann, and M. Weis, *Phys. Rev. Lett.* **41**, 469 (1978).
 [10] M. Schadel, W. Bruchle, H. Gaggeler, J. V. Kratz, K. Summerer, G. Wirth, G. Herrmann, R. Stakemann, G. Tittel, N. Trautmann, J. M. Nitschke, E. K. Hulet, R. W. Loughheed, R. L. Hahn, and R. L. Ferguson, *Phys. Rev. Lett.* **48**, 852 (1982).
 [11] K. J. Moody, D. Lee, R. B. Welch, K. E. Gregorich, G. T. Seaborg, R. W. Loughheed, and E. K. Hulet, *Phys. Rev. C* **33**, 1315 (1986).
 [12] D. Lee, K. J. Moody, M. J. Nurmia, G. T. Seaborg, H. R. von Gunten, and D. C. Hoffman, *Phys. Rev. C* **27**, 2656 (1983).
 [13] D. C. Hoffman, M. M. Fowler, W. R. Daniels, H. R. von Gunten, D. Lee, K. J. Moody, K. Gregorich, R. Welch, G. T. Seaborg, W. Bruchle, M. Brugger, H. Gaggeler, M. Schadel, K. Summerer, G. Wirth, T. Blaich, G. Herrmann, N. Hildebrand, J. V. Kratz, M. Lerch, and N. Trautmann, *Phys. Rev. C* **31**, 1763 (1985).
 [14] A. Turler, H. R. von Gunten, J. D. Leyba, D. C. Hoffman, D. M. Lee, K. E. Gregorich, D. A. Bennett, R. M. Chasteler, C. M. Gannett, H. L. Hall, R. A. Henderson, and M. J. Nurmia, *Phys. Rev. C* **46**, 1364 (1992).
 [15] J. V. Kratz, M. Schädel, and H. W. Gäggeler, *Phys. Rev. C* **88**, 054615 (2013).
 [16] W. D. Loveland, *Front. Phys.* **7**, 23 (2019).
 [17] V. I. Zagrebaev and W. Greiner, *J. Phys. G: Nucl. Part. Phys.* **34**, 2265 (2007).
 [18] V. Zagrebaev and W. Greiner, *Phys. Rev. Lett.* **101**, 122701 (2008).
 [19] V. I. Zagrebaev and W. Greiner, *Phys. Rev. C* **83**, 044618 (2011).
 [20] G. G. Adamian, N. V. Antonenko, and A. S. Zubov, *Phys. Rev. C* **71**, 034603 (2005).
 [21] G. G. Adamian, N. V. Antonenko, V. V. Sargsyan, and W. Scheid, *Phys. Rev. C* **81**, 024604 (2010).
 [22] K. Zhao, Z. Li, N. Wang, Y. Zhang, Q. Li, Y. Wang, and X. Wu, *Phys. Rev. C* **92**, 024613 (2015).
 [23] C. Li, F. Zhang, J. Li, L. Zhu, J. Tian, N. Wang, and F. S. Zhang, *Phys. Rev. C* **93**, 014618 (2016).
 [24] N. Wang and L. Guo, *Phys. Lett. B* **760**, 236 (2016).
 [25] K. Zhao, Z. Liu, F. S. Zhang, and N. Wang, *Phys. Lett. B* **815**, 136101 (2021).
 [26] L. Zhu, J. Su, W. J. Xie, and F. S. Zhang, *Phys. Rev. C* **94**, 054606 (2016).
 [27] Z. Q. Feng, *Phys. Rev. C* **95**, 024615 (2017).
 [28] L. Zhu, J. Su, W. J. Xie, and F. S. Zhang, *Phys. Lett. B* **767**, 437 (2017).
 [29] K. Sekizawa and K. Yabana, *Phys. Rev. C* **88**, 014614 (2013).
 [30] K. Sekizawa, *Phys. Rev. C* **96**, 041601(R) (2017).
 [31] K. Godbey, C. Simenel, and A. S. Umar, *Phys. Rev. C* **101**, 034602 (2020).
 [32] X. Jiang and N. Wang, *Phys. Rev. C* **101**, 014604 (2020).
 [33] V. Zagrebaev and W. Greiner, *J. Phys. G: Nucl. Part. Phys.* **31**, 825 (2005).
 [34] P. H. Chen, F. Niu, and Z. Q. Feng, *Phys. Rev. C* **102**, 014621 (2020).
 [35] V. I. Zagrebaev and W. Greiner, *Nucl. Phys. A* **944**, 257 (2015).
 [36] Z. Q. Feng, G. M. Jin, and J. Q. Li, *Phys. Rev. C* **80**, 067601 (2009).
 [37] A. V. Karpov and V. V. Saiko, *Phys. Rev. C* **96**, 024618 (2017).
 [38] Z. J. Wu and L. Guo, *Phys. Rev. C* **100**, 014612 (2019).
 [39] Yu. E. Penionzhkevich, G. G. Adamian, and N. V. Antonenko, *Eur. Phys. J. A* **27**, 187 (2006).
 [40] S. Ayik, B. Yilmaz, O. Yilmaz, and A. S. Umar, *Phys. Rev. C* **100**, 014609 (2019).
 [41] S. Ayik, B. Yilmaz, O. Yilmaz, A. S. Umar, and G. Turan, *Phys. Rev. C* **96**, 024611 (2017).
 [42] S. Ayik, B. Yilmaz, O. Yilmaz, and A. S. Umar, *Phys. Rev. C* **97**, 054618 (2018).
 [43] P. W. Wen, A. K. Nasirov, C. J. Lin, and H. M. Jia, *J. Phys. G: Nucl. Part. Phys.* **47**, 075106 (2020).
 [44] X. Jiang and N. Wang, *Chin. Phys. C* **42**, 104105 (2018).
 [45] C. Li, C. A. T. Sokhna, X. Xu, J. Li, G. Zhang, B. Li, Z. Ge, and F.-S. Zhang, *Phys. Rev. C* **99**, 034619 (2019).
 [46] A. Winther, *Nucl. Phys. A* **572**, 191 (1994); **594**, 203 (1995).
 [47] X. J. Bao, *Phys. Rev. C* **102**, 054613 (2020); **102**, 064604 (2020).

- [48] X. J. Bao, S. Q. Guo, H. F. Zhang, and J. Q. Li, *Phys. Rev. C* **97**, 024617 (2018).
- [49] X. J. Bao, S. Q. Guo, H. F. Zhang, and J. Q. Li, *Phys. Lett. B* **785**, 221 (2018).
- [50] X. J. Bao, *Nucl. Phys. A* **986**, 60 (2019).
- [51] X. J. Bao, *Phys. Rev. C* **100**, 011601(R) (2019).
- [52] S. Q. Guo, X. J. Bao, H. F. Zhang, J. Q. Li, and N. Wang, *Phys. Rev. C* **100**, 054616 (2019).
- [53] G. Wolschin and W. Nörenberg, *Z. Phys. A* **284**, 209 (1978).
- [54] C. Riedel, G. Wolschin, and W. Norenberg, *Z. Phys. A* **290**, 47 (1979).
- [55] X. J. Bao, *Chin. Phys. C* **43**, 054105 (2019).
- [56] X. J. Bao, *Phys. Rev. C* **104**, 034604 (2021).
- [57] G. G. Adamian *et al.*, *Int. J. Mod. Phys. E* **05**, 191 (1996).
- [58] Q. Li, W. Zuo, W. Li *et al.*, *Eur. Phys. J. A* **24**, 223 (2005).
- [59] C. Y. Wong, *Phys. Rev. Lett.* **31**, 766 (1973).
- [60] N. Wang, M. Liu, and X. Wu, *Phys. Rev. C* **81**, 044322 (2010).
- [61] R. J. Charity, *Phys. Rev. C* **82**, 014610 (2010).
- [62] D. Mancusi, R. J. Charity, and J. Cugnon, *Phys. Rev. C* **82**, 044610 (2010).
- [63] R. Bass, *Phys. Rev. Lett.* **39**, 265 (1977).
- [64] R. B. Welch, K. J. Moody, K. E. Gregorich, D. Lee, and G. T. Seaborg, *Phys. Rev. C* **35**, 204 (1987).
- [65] R. Yanez and W. Loveland, *Phys. Rev. C* **91**, 044608 (2015).